

Gap generation and phase diagram in strained graphene in a magnetic field

D.O. Rybalka,¹ E.V. Gorbar,^{1,2} and V.P. Gusynin²

¹*Department of Physics, Taras Shevchenko National Kiev University, 03022, Kiev, Ukraine*

²*Bogolyubov Institute for Theoretical Physics, 03680, Kiev, Ukraine*

(Dated: November 5, 2018)

The gap equation for Dirac quasiparticles in monolayer graphene in constant magnetic and pseudomagnetic fields, where the latter is due to strain, is studied in a low-energy effective model with contact interactions. Analyzing solutions of the gap equation, the phase diagram of the system in the plane of pseudomagnetic and parallel magnetic fields is obtained in the approximation of the lowest Landau level. The three quantum Hall states, ferromagnetic, antiferromagnetic, and canted antiferromagnetic, are realized in different regions of the phase diagram. It is found that the structure of the phase diagram is sensitive to signs and values of certain four-fermion interaction couplings which break the approximate spin-value $SU(4)$ symmetry of the model.

I. INTRODUCTION

Among many remarkable properties of graphene its response to strain can be singled out as one of efficient means to change and control the characteristics of the electronic states in graphene. Since graphene is only one atom thick, it is easily subjected to mechanical deformations. Various proposals to engineer strain in graphene were discussed in the literature¹⁻³. It is known that strain induces effective gauge fields^{4,5} with the corresponding effective "magnetic" fields of opposite sign in valleys K and K' that means that elastic deformations, unlike real magnetic field, preserve time reversal symmetry^{6,7}. Since time reversal symmetry is unbroken, strain induced fields are known as pseudomagnetic fields in the literature (for a review of gauge fields in strained graphene, see Refs.[8,9]). It was proposed in Refs.[10,11] that a designed strain may induce uniform pseudomagnetic field, which can easily reach values exceeding 10 T.

The observation of anomalous integer quantum Hall (QH) effect with the filling factors $\nu = \pm 4(|n| + 1/2)$ (n is the Landau level index) in graphene in a magnetic field¹², in accordance with theoretical studies in Refs.[13,14], was a milestone in graphene research as it became a direct experimental proof of the existence of gapless Dirac quasiparticles in graphene. The four-fold degeneracy of the Landau levels in graphene is due to the $SU(4)$ symmetry connected with valley and spin. Later the plateaus $\nu = 0, \pm 1, \pm 4$ in the QH effect in graphene were observed^{15,16} in a strong magnetic field $B \geq 20T$. These plateaus are connected with the magnetic field induced splitting of the $n = 0$ and $n = 1$ Landau levels and the degeneracy of the lowest Landau level (LLL) is thus completely resolved.

The Landau levels related to pseudomagnetic fields^{10,11} were observed in spectroscopic measurements.¹⁷ It was pointed out¹⁸ that pseudomagnetic fields due to strain can interfere in many ways with real magnetic fields. For example, the interplay of pseudomagnetic and magnetic fields in the quantum Hall regime causes backscattering in the chiral edge channels that can destroy the quantized conductance plateaus and gives rise to unconventional QH effect in strained graphene¹⁹ with oscillating Hall conductivity.

The gap generation in graphene in the presence of a pseudomagnetic field was studied in Ref.[20]. Interestingly, it was found that unlike magnetic field which catalyses the generation of the time reversal invariant Dirac mass, pseudomagnetic field catalyses the generation of time-reversal symmetry breaking Haldane mass. Various competing ground states in monolayer graphene in pseudomagnetic fields were recently studied in Ref.[21]. Finally, we would like to add that very strong 50 – 60 T pseudomagnetic fields may be realized in molecular graphene²².

The interplay between different possible ground states in strained graphene in a magnetic field represents an important unsolved problem at the moment. In the present paper, we study a gap generation for quasiparticles in monolayer graphene in the presence of both constant magnetic and pseudomagnetic fields and using the model with local four-fermion interactions considered in Refs.[23,24]. Local four-fermion terms in the Hamiltonian are remnants of the interactions on the atomic scale, and in spite being much smaller than Coulomb interaction, they play an important role in deciding how the $SU(4)$ symmetry is broken in monolayer graphene as well as bilayer graphene. This especially concerns the nature of the QH state with half-filled zero-energy Landau level. We obtain the phase diagram for competing quantum Hall states in the LLL approximation when the chemical potential is tuned to the charge neutrality point, i.e., the state with the zero filling factor.

The paper is organized as follows. We begin by presenting in Sec.II the model describing low-energy quasiparticles excitations in strained monolayer graphene in an external magnetic field and in the presence of local four-fermion interactions. The derivation of the gap equation is given in Sec.III and its solutions are presented in Sec.IV. The phase diagram of the system is derived and discussed in Sec.V. The main results are summarized in Sec.VI. Appendices at the end of the paper contain technical details and derivations used to supplement the presentation in the main text.

II. HAMILTONIAN OF THE MODEL

The low-energy quasiparticles excitations in graphene can be described in terms of a four-component Dirac spinor $\Psi_\alpha^T = (\psi_{KA\alpha}, \psi_{KB\alpha}, \psi_{K'B\alpha}, \psi_{K'A\alpha})$ which combines the Bloch states with spin index $\alpha = 1, 2$ on the two different sublattices (A, B) and with momenta near the two nonequivalent valley points (K, K') of the Brillouin zone. The free quasiparticle Hamiltonian has a relativistic-like form with the Fermi velocity $v_F = 10^6 m/s$ playing the role of the speed of light

$$H_0 = \int d^2r [v_F \bar{\Psi}(\gamma^1 \pi_x + \gamma^2 \pi_y) \Psi + \epsilon_Z \Psi^\dagger \sigma_z \Psi], \quad (1)$$

where $\bar{\Psi} = \Psi^\dagger \gamma^0$ is the Dirac conjugated spinor and $\mathbf{r} = (x, y)$. The matrices γ^ν with $\nu = 0, 1, 2$ are 4×4 matrices which satisfy the anticommutation relations of the Dirac algebra $\{\gamma^\mu, \gamma^\nu\} = 2g^{\mu\nu}$, where $g^{\mu\nu} = \text{diag}(1, -1, -1)$ and $\mu, \nu = 0, 1, 2$. These matrices belong to a reducible representation of the Dirac algebra $\gamma^\nu = \tilde{\tau}_z \otimes (\tau_z, i\tau_y, -i\tau_x)$, where the Pauli matrices $\tilde{\tau}_i$ and τ_i with $i = x, y, z$ act in the subspaces of the valley (K, K') and sublattices (A, B) indices, respectively.

The canonical momentum $\boldsymbol{\pi} = -i\hbar\nabla + e\mathbf{A}/c + \gamma^3\gamma^5 e\mathbf{A}_5/c$ includes the vector potential in the Landau gauge $\mathbf{A} = (0, B_\perp x)$ corresponding to the component \mathbf{B}_\perp of an external magnetic field \mathbf{B} orthogonal to the plane of graphene, and \mathbf{A}_5 is the vector potential describing the strain induced gauge fields^{19,20,25,26}. In the representation of the Dirac matrices that we use, γ^3 and $\gamma^5 = i\gamma^0\gamma^1\gamma^2\gamma^3$ matrices equal $\gamma^3 = i\tilde{\tau}_y \otimes I$ and $\gamma^5 = \tilde{\tau}_x \otimes I$, where I is the 2×2 unit matrix. It is easy to check that the product of these matrices $\gamma^3\gamma^5 = \tilde{\tau}_z \otimes I$ is a matrix diagonal in the subspace of valleys that ensures that the term in the canonical momentum with the vector potential \mathbf{A}_5 takes opposite signs in K and K' valleys. In what follows, we will consider only the case of constant magnetic \mathbf{B} and pseudomagnetic \mathbf{B}_5 fields. The pseudomagnetic field \mathbf{B}_5 points always in the direction perpendicular to the plane of graphene and, therefore, is described by the vector potential $\mathbf{A}_5 = (0, B_5 x)$, where $B_5 = |\mathbf{B}_5|$.

The last term in the free Hamiltonian (1) is the Zeeman interaction $\epsilon_Z = \mu_B B$ with $\mu_B = e\hbar/(2mc)$ being the Bohr magneton and σ_z is Pauli spin matrix whose eigenstates describe spin states directed along or against the magnetic field \mathbf{B} . Here $B = \sqrt{\mathbf{B}_\perp^2 + \mathbf{B}_\parallel^2}$ is the strength of the magnetic field and \mathbf{B}_\parallel is its component parallel to the plane of graphene. We note that the standard Zeeman interaction $\mu_B \mathbf{B} \boldsymbol{\sigma}$ can be reduced to this form using a rotation in spin space.

The Coulomb interaction between electrons is described by the following Hamiltonian:

$$H_C = \frac{1}{2} \int d^2r d^2r' \bar{\Psi}(\mathbf{r}) \gamma^0 \Psi(\mathbf{r}) U_C(\mathbf{r} - \mathbf{r}') \bar{\Psi}(\mathbf{r}') \gamma^0 \Psi(\mathbf{r}'),$$

where $U_C(\mathbf{r})$ is the Coulomb potential. In order to simplify the analysis, we follow the approach of Ref.[27] and replace the Coulomb interaction $U_C(\mathbf{r})$ by the contact interaction $G_{int} \delta^2(\mathbf{r})$. The Hamiltonian $H_0 + H_C$ in the absence of the Zeeman term possesses a global $SU(4)$ symmetry connected with valley and spin degrees of freedom.

Although the Coulomb interaction is the strongest interaction between electrons in graphene, local four-fermion interactions^{28,29} play a crucial role too. Although these interactions are much smaller than the Coulomb one, they break, in general, the $SU(4)$ symmetry and crucially affect the selection of the ground state of the system. A set of local valley and sublattice asymmetric four-fermion interactions was introduced in Ref.[23]. The $\nu = 0$ quantum Hall state was studied and it was shown that the phase diagram, obtained in the presence of generic valley and sublattice anisotropy and the Zeeman interaction, consists of four phases: ferromagnetic, canted antiferromagnetic (CAF), charge density wave, and Kekule distortion. The Hamiltonian of generic local four-fermion interactions reads

$$H_{contact} = \frac{1}{2} \int d^2r \sum_{j,k} g_{jk} [\bar{\Psi}(\mathbf{r}) \gamma^0 \mathcal{T}_{jk} \Psi(\mathbf{r})]^2, \quad \mathcal{T}_{jk} = \tilde{\tau}_j \otimes \tau_k, \quad (2)$$

where $j, k = x, y, z$. We do not include in $H_{contact}$ the term with g_{00} as it corresponds to the local Coulomb interaction, which has already been taken into account by G_{int} . In addition, we do not include in our model the terms with g_{0k} and g_{j0} , which vanish in the first order in the Coulomb interactions and arise only in the second order due to virtual transitions to other bands²³. The coupling constants g_{jk} are not all independent. As shown in Ref.[23], symmetry and other considerations lead to the following equalities for nonzero constants:

$$g_{\perp\perp} = g_{xx} = g_{xy} = g_{yx} = g_{yy}, \quad g_{\perp z} = g_{xz} = g_{yz}, \quad g_{z\perp} = g_{zx} = g_{zy}. \quad (3)$$

Thus, totally we have four interaction coupling constants, $G_{int}, g_{\perp\perp}, g_{\perp z}, g_{z\perp}$, in the considered model. Finally, let

us present \mathcal{T}_{jk} in terms of the γ -matrices

$$\begin{aligned}\mathcal{T}_{xx} &= -i\gamma^3\gamma^2, & \mathcal{T}_{xy} &= i\gamma^3\gamma^1, & \mathcal{T}_{xz} &= -\gamma^3\gamma^0, \\ \mathcal{T}_{yx} &= -\gamma^5\gamma^2, & \mathcal{T}_{yy} &= \gamma^5\gamma^1, & \mathcal{T}_{yz} &= i\gamma^5\gamma^0, \\ \mathcal{T}_{zx} &= i\gamma^2, & \mathcal{T}_{zy} &= -i\gamma^1, & \mathcal{T}_{zz} &= \gamma^0.\end{aligned}\quad (4)$$

All these matrices are normalized as $\mathcal{T}_{ij}^2 = 1$. This presentation is useful for the derivation of the gap equation in the next section.

III. GAP EQUATION

We will solve the gap equation in the Hartree-Fock (mean-field) approximation^{30–33} which is conventional and appropriate in this case. In the subsection III A, we will derive the gap equation in the case where only real magnetic field is present. In the next subsection, we will generalize the gap equation to the case where both magnetic and pseudomagnetic fields are present.

A. Magnetic field

At zero temperature and in the clean limit (no impurities), the Schwinger-Dyson equation for the quasiparticle propagator $G(u, u') = \hbar^{-1}\langle 0|T\Psi(u)\bar{\Psi}(u')|0\rangle$ in graphene in the mean-field approximation takes the form

$$\begin{aligned}iG^{-1}(u, u') &= iS^{-1}(u, u') - \hbar G_{int}\gamma^0 G(u, u)\gamma^0\delta(u - u') + \hbar G_{int}\gamma^0\text{tr}[\gamma^0 G(u, u)]\delta(u - u') \\ &\quad - \hbar \sum_{j,k} g_{jk}\{\gamma^0\mathcal{T}_{jk}G(u, u)\gamma^0\mathcal{T}_{jk} - \gamma^0\mathcal{T}_{jk}\text{tr}[\gamma^0\mathcal{T}_{jk}G(u, u)]\}\delta(u - u'),\end{aligned}\quad (5)$$

where $u = (t, \mathbf{r})$. In this subsection, we will derive the gap equation in graphene in a magnetic field. The generalization to the case of both magnetic and pseudomagnetic fields is rather straightforward and will be considered in the next subsection.

The inverse free propagator in the case under consideration is given by

$$iS^{-1}(u, u') = [(i\hbar\partial_t - \epsilon_Z\sigma_z)\gamma^0 - v_F(\boldsymbol{\pi} \cdot \boldsymbol{\gamma})]\delta(u - u').\quad (6)$$

For the full quasiparticle propagator, we will use an ansatz which is a generalization of the ansatz used in the previous work by two of us²⁷

$$iG^{-1}(u, u') = [i\hbar\partial_t\gamma^0 + \mu\gamma^0 + \tilde{\mu}\gamma^0\gamma^3\gamma^5 - v_F(\boldsymbol{\pi} \cdot \boldsymbol{\gamma}) - \tilde{\Delta} + \Delta\gamma^3\gamma^5]\delta(u - u'),\quad (7)$$

where matrices $\mu, \tilde{\mu}, \Delta, \tilde{\Delta}$ are defined as $\mu = \mu_\nu\sigma_\nu, \tilde{\mu} = \tilde{\mu}_\nu\sigma_\nu, \Delta = \Delta_\nu\sigma_\nu, \tilde{\Delta} = \tilde{\Delta}_\nu\sigma_\nu$, and index ν runs the values $\nu = 0, x, z$ with σ_x and σ_z being Pauli spin matrices and σ_0 the unit 2×2 matrix [the absence of quantities with σ_y matrix is consistent with subsequent analysis of a gap equation]. In what follows, we consider twelve dynamically generated parameters $\mu_\nu, \tilde{\mu}_\nu, \Delta_\nu$, and $\tilde{\Delta}_\nu$ as constant that is consistent with our mean-field analysis of the present model with contact interactions.

The parameters μ_j and $\tilde{\mu}_j$ with $j = x, z$ are generalized chemical potentials connected with the QH ferromagnetism^{28,32–34}. On the other hand, Δ_j and $\tilde{\Delta}_j$ are related to the magnetic catalysis scenario^{35–38} and are Haldane and Dirac masses, respectively, and correspond to excitonic condensates (for a brief review of the QH ferromagnetism and magnetic catalysis scenario, see Refs.[39–41]). Actually, it was shown in Ref.[27] that the QH ferromagnetism and magnetic catalysis scenario order parameters necessarily coexist. The physics underlying their coexistence is specific for the systems with relativistic-like quasiparticle spectrum that makes the quantum Hall dynamics of the $SU(4)$ breakdown in graphene to be quite different from that in conventional systems with non-relativistic quasiparticle spectrum.

According to Eq.(7), the full propagator $G(u, u')$ can be written in the form

$$G(u, u') = i\langle u| \left[(i\hbar\partial_t + \mu)\gamma^0 - v_F(\boldsymbol{\pi} \cdot \boldsymbol{\gamma}) + i\tilde{\mu}\gamma^1\gamma^2 + i\Delta\gamma^0\gamma^1\gamma^2 - \tilde{\Delta} \right]^{-1} |u'\rangle,\quad (8)$$

where the states $|u\rangle$ are eigenstates of the time-position operator \hat{u} : $\hat{u}|u\rangle = u|u\rangle$, $\langle u|u'\rangle = \delta(u - u')$. In Appendix A, we derive an explicit expression for the propagator $G(u, u')$ in the form of a sum over Landau levels.

The symmetry-breaking generalized chemical potentials and gaps $\mu_\nu, \tilde{\mu}_\nu, \Delta_\nu, \tilde{\Delta}_\nu$ are related to the corresponding order parameters through the following relationship:

$$\langle \bar{\Psi} \mathcal{O}_\nu \Psi \rangle = -\hbar \text{tr}[\mathcal{O}_\nu G(u, u)], \quad (9)$$

where 8×8 matrices $\mathcal{O}_\nu = \gamma^0 \sigma_\nu, \gamma^0 \gamma^3 \gamma^5 \sigma_\nu, \gamma^3 \gamma^5 \sigma_\nu, \sigma_\nu$, respectively. Compared to our previous analysis,^{27,42} we included the spin matrix σ_x in order to be able to describe the canted antiferromagnetic state.

Since the right-hand side of the gap equation (5) contains the full propagator at the coincidence limit $u' = u$, we should calculate $G(u, u')|_{u=u'} = \bar{G}(u, u)$, where \bar{G} is the translation invariant part of the full propagator defined in the mixed frequency-momentum representation in Eq.(A15). By making use of Eqs. (A19) and (A20), we find that

$$G(u, u) = \int_{-\infty}^{\infty} \frac{d\omega d^2k}{(2\pi)^3 \hbar} \bar{G}(\omega, \mathbf{k}) = \frac{i}{2\pi l^2} \sum_{n=0}^{\infty} \int_{-\infty}^{\infty} \frac{d\omega}{2\pi \hbar} W \frac{[P_- + P_+ \theta(n-1)]}{M - n\epsilon_B^2}, \quad (10)$$

where $l = \sqrt{\hbar c / |eB_\perp|}$ is the magnetic length, $\epsilon_B = \sqrt{2\hbar v_F^2 |eB_\perp| / c} \simeq 424 \sqrt{|B_\perp| [\text{T}]} \text{K}$ is the Landau energy scale, P_\pm are projectors given by Eq.(A11), and W, M are matrices expressed through $\mu, \tilde{\mu}, \Delta, \tilde{\Delta}$ and defined in Eqs.(A2) and (A3). We note that the filling factor $\nu = 2\pi l^2 \rho$ is related to the carrier imbalance $\rho = n_e - n_h$, where n_e and n_h are the densities of electrons and holes, respectively, and ρ is determined through the Green's function as

$$\rho = \langle 0 | \Psi^\dagger(u) \Psi(u) | 0 \rangle = -\hbar \text{tr}[\gamma^0 G(u, u)]. \quad (11)$$

Since W and M contain only γ^0 and $\gamma^1 \gamma^2$ Dirac matrices, it is convenient to work with eigenvectors of these matrices. The equality $(\gamma^1 \gamma^2)^2 = -1$ implies that the eigenvectors $|s_{12}\rangle$ of the matrix $\gamma^1 \gamma^2$ are purely imaginary

$$\gamma^1 \gamma^2 |s_{12}\rangle = i s_{12} |s_{12}\rangle, \quad s_{12} = \pm 1. \quad (12)$$

Similarly, since $(\gamma^0)^2 = 1$, the eigenvectors of the matrix γ^0 are real and given by

$$\gamma^0 |s_0\rangle = s_0 |s_0\rangle, \quad s_0 = \pm 1. \quad (13)$$

Furthermore, since γ^0 and $\gamma^1 \gamma^2$ commute, we can consider states $|s_0 s_{12}\rangle$ which are simultaneously eigenvectors of γ^0 and $\gamma^1 \gamma^2$ with eigenvalues s_0 and $i s_{12}$, respectively. The vectors $|s_0 s_{12}\rangle$ form a complete basis, and since W and M contain only γ^0 and $\gamma^1 \gamma^2$ matrices, the propagator $G(u, u)$ is diagonal in the basis of $|s_{12} s_0\rangle$ vectors and is given by

$$G(u, u; s_0, s_{12}) = \frac{i}{4\pi l^2} \int_{-\infty}^{\infty} \frac{d\omega}{2\pi \hbar} \sum_{n=0}^{\infty} [s_0(\omega + m) + d] [c_0 + c_j \sigma_j]^{-1} \\ \times \left(1 + s_{12} s_\perp + [1 - s_{12} s_\perp] \theta(n - 1/2) \right), \quad j = x, y, z. \quad (14)$$

Here $s_\perp = \text{sgn}(eB_\perp)$, the matrices m and d are defined in Appendix A, and the coefficients c_0, c_j are

$$c_0 = \omega^2 + 2\omega m_0 - n\epsilon_B^2 + m_\nu^2 - d_\nu^2, \quad c_y = 2i s_0 (d_x m_z - d_z m_x), \quad (15)$$

$$c_x = 2(\omega m_x + m_0 m_x - d_0 d_x), \quad c_z = 2(\omega m_z + m_0 m_z - d_0 d_z), \quad (16)$$

where $m_\nu = \mu_\nu - s_0 s_{12} \tilde{\mu}_\nu$, $d_\nu = \tilde{\Delta}_\nu + s_0 s_{12} \Delta_\nu$ ($\nu = 0, x, z$) and summation over dummy index ν is meant. For strong magnetic fields, we write

$$G(u, u) = G_{LLL}(u, u) + G_{hLL}(u, u), \quad (17)$$

where we separated the contributions of the zero Landau level, $G_{LLL}(u, u)$ with $n = 0$, and higher Landau levels, $G_{hLL}(u, u)$ with $n \geq 1$, in Eq.(14).

Let us calculate first the lowest Landau level propagator $G_{LLL}(u, u)$. In order to integrate over ω in Eq.(14), we rewrite the integrand by using the relation

$$c_0 + c_j \sigma_j = [s_0(\omega + m) - d] [s_0(\omega + m) + d] \quad (18)$$

valid for $n = 0$ and assume as usual that ω is replaced by $\omega + i\epsilon \text{sgn} \omega$ and $\epsilon \rightarrow 0_+$. Hence we obtain that Eq.(14) implies the following propagator at the limit of coinciding points in the LLL approximation:

$$G_{LLL}(u, u; s_0, s_{12}) = \frac{i}{2\pi l^2} \frac{1 + s_{12} s_\perp}{2} \int_{-\infty}^{\infty} \frac{d\omega}{2\pi \hbar} (s_0 \omega + s_0 m_\nu \sigma_\nu - d_\nu \sigma_\nu)^{-1} \\ = -\frac{s_0}{4\pi \hbar l^2} \frac{1 + s_{12} s_\perp}{2} \left[\frac{(m_i - s_0 d_i) \sigma_i}{E} \theta(E - |\mu_L|) + \text{sgn}(\mu_L) \theta(|\mu_L| - E) \right], \quad i = x, z \quad (19)$$

where the factor $(1 + s_{12}s_{\perp})/2$ with $s_{\perp} = \text{sgn}(eB_{\perp})$ reflects the presence of the spin projector $P_{-} = (1 - is_{\perp}\gamma^1\gamma^2)/2$ in the LLL contribution, energy

$$E = \sqrt{(m_x - s_0d_x)^2 + (m_z - s_0d_z)^2}, \quad (20)$$

and we introduced the notation

$$\mu_L = m_0 - s_0d_0 = \mu_0 - s_0s_{12}\tilde{\mu}_0 - s_0\tilde{\Delta}_0 - s_{12}\Delta_0 \quad (21)$$

for an "effective chemical potential" in the lowest Landau level.

By integrating over ω , it is not difficult to check that the higher Landau level contribution $G_{hLL}(u, u)$ diverges as $\sum_{n=1}^{\infty} n^{-1/2}$. Indeed, making the change of the variable $\omega \rightarrow \sqrt{n}\epsilon_B\omega$ and taking into account that all the dynamically generated parameters are much less than the scale ϵ_B , we find that the leading contribution at large $n\epsilon_B^2$ is given by

$$G_{hLL}(u, u; s_0, s_{12}) \simeq \frac{1}{4\pi\hbar l^2} \sum_{n=1}^{\infty} \frac{1}{\sqrt{n}} \frac{d_{\nu}\sigma_{\nu}}{\epsilon_B}. \quad (22)$$

This means that the right-hand side of the gap equation (5) diverges too. This result is the well-known artefact of using a model with local four-fermion interactions. For a long-range interaction like, for example, the Coulomb one considered in Ref.[42], such a divergence is absent because the gap equation contains the quasiparticle propagator at different points u and u' . To proceed further, we regularize the divergence in the model under consideration introducing a cutoff n_{max} in the sum over Landau levels (a slightly different approach was used in Ref.[27]), which is connected with the ultraviolet (UV) cut-off in energy Λ (band width) according to the relation $n_{max} = \Lambda^2/\epsilon_B^2$. By using the regularization described above and retaining only the leading contribution, we find that the higher Landau levels contribution to the propagator at the limit of coinciding points is given by

$$G_{hLL}(u, u; s_0, s_{12}) = \frac{\Lambda}{4\pi\hbar^3v_F^2} d_{\nu}\sigma_{\nu}. \quad (23)$$

By combining Eqs.(23) and (19), the gap equation (5) takes the following final form:

$$\begin{aligned} s_0m_{\nu}\sigma_{\nu} - d_{\nu}\sigma_{\nu} + s_0s_{\perp}\epsilon_Z\sigma_z = & - (G_{int} + g_{zz})G(s_0, s_{12}) - 4g_{\perp\perp}G(s_0, -s_{12}) + 2g_{z\perp}G(-s_0, -s_{12}) \\ & + 2g_{\perp z}G(-s_0, s_{12}) + g_{zz} \sum_{s'_0, s'_{12}} \text{tr} G(s'_0, s'_{12}), \end{aligned} \quad (24)$$

where

$$\begin{aligned} G(s_0, s_{12}) & \equiv G_{LLL}(u, u; s_0, s_{12}) + G_{hLL}(u, u; s_0, s_{12}) \\ & = \frac{-s_0}{4\pi\hbar l^2} \left[\frac{(m_i - s_0d_i)\sigma_i}{E} \theta(E - |\mu_L|) + \text{sgn}(\mu_L) \theta(|\mu_L| - E) \right] \frac{1 + s_{12}s_{\perp}}{2} + \frac{\Lambda}{4\pi\hbar^3v_F^2} d_{\nu}\sigma_{\nu}, \end{aligned} \quad (25)$$

and trace in the last term in Eq.(24) is taken over the Pauli spin matrices [note that the quantities E and μ_L depend on s_0, s_{12} according to Eqs.(20),(21) and m_{ν}, d_{ν} depend on them too]. In deriving Eq.(24), we omitted the third term on the right-hand side of Eq.(5) which defines the Hartree contribution due to the charge density of carriers. The point is that there are other contributions due to the charges of ions in graphene and the charges in the substrate and gates. In view of the overall neutrality of the system, all these contributions should cancel exactly (the Gauss law).

Finally, we would like to note that it is advantageous in deriving Eq.(24) to use T_{jk} matrices given by Eq.(4) and utilize the Dirac algebra in order to calculate the contribution to the gap equation due to the last term in Eq.(5). [The matrices T_{jk} have simple commutation relations with the Green's function $G(u, u)$ which contains only γ^0 and $\gamma^1\gamma^2$ matrices (see Eq.(10)).]

B. Magnetic and pseudomagnetic fields

In this subsection, we will derive the gap equation for quasiparticles in graphene in the case where both constant magnetic and pseudomagnetic fields are present. Then the canonical momentum has the form $\boldsymbol{\pi} = -i\hbar\nabla + e\mathbf{A}/c + \gamma^3\gamma^5 e\mathbf{A}_5/c$, where $\mathbf{A} = (0, B_{\perp}x)$ and $\mathbf{A}_5 = (0, B_5x)$. Repeating the same computations as in the previous subsection, one can show that the only difference between the former and present cases is that the magnetic field B_{\perp} is now replaced by the effective field $B_{\perp} + (i\gamma^0\gamma^1\gamma^2)B_5$ or $B_{\perp} - s_0s_{12}B_5$ in the eigenstate basis of the matrices γ^0 and $\gamma^1\gamma^2$.

Consequently, the pseudomagnetic field has opposite signs in the K and K' valleys. Therefore, in order to take into account pseudomagnetic field, we should simply make the replacement $B_{\perp} \rightarrow B_{\perp} - s_0 s_{12} B_5$ in the corresponding equations of Subsec.III A except the Zeeman energy, where $\epsilon_Z = \mu_B \sqrt{B_{\perp}^2 + B_{\parallel}^2}$, which includes the component of the magnetic field parallel to the plane of graphene. We find it convenient in the analysis below to use the notation $b_{\parallel} = B_{\parallel}/B_{\perp}$ and $b_5 = B_5/B_{\perp}$.

Taking into account all Landau levels contributions, the gap equation for quasiparticles in graphene in the presence of constant magnetic and pseudomagnetic fields is given by

$$s_0 m_{\nu} \sigma_{\nu} - d_{\nu} \sigma_{\nu} + s_0 s_{\perp} \epsilon_Z \sigma_z = - (G_{int} + g_{zz}) G^{(5)}(s_0, s_{12}) - 4g_{\perp\perp} G^{(5)}(s_0, -s_{12}) \\ + 2g_{z\perp} G^{(5)}(-s_0, -s_{12}) + 2g_{\perp z} G^{(5)}(-s_0, s_{12}) + g_{zz} \sum_{s'_0, s'_{12}} \text{tr} G^{(5)}(s'_0, s'_{12}), \quad (26)$$

where

$$G^{(5)}(s_0, s_{12}) = \frac{-s_0 |eB_{\perp} - s_0 s_{12} eB_5|}{4\pi \hbar^2 c} \left[\frac{(m_i - s_0 d_i) \sigma_i}{E} \theta(E - |\mu_L|) + \text{sgn}(\mu_L) \theta(|\mu_L| - E) \right] \\ \times \frac{1 + s_{12} \text{sgn}(eB_{\perp} - s_0 s_{12} eB_5)}{2} + \frac{\Lambda}{4\pi \hbar^3 v_F^2} d_{\nu} \sigma_{\nu}. \quad (27)$$

The first term on the right-hand side of Eq.(27) is the LLL contribution and the last one describes the contribution due to higher Landau levels.

We have found solutions of the gap equation taking into account the contributions due to all Landau levels. It turned out that the higher Landau levels contribution in the weak coupling regime does not qualitatively change the results obtained in strong magnetic fields when the LLL approximation is valid. On the other hand, the higher Landau levels contribution essentially enlarges formulas and makes them very complicated. Therefore, in what follows, we will solve the gap equation and present our analysis in the LLL approximation omitting the contribution due to higher Landau levels.

IV. SOLUTIONS OF GAP EQUATION IN THE LLL APPROXIMATION

In this section, we consider solutions of the gap equation (26) retaining only the LLL contribution. Propagator (27) in the LLL approximation contains different projectors depending on which field B_{\perp} or B_5 is stronger. We will consider both possibilities separately.

A. $|B_{\perp}| > |B_5|$

Let us find solutions of the gap equation (26) in the LLL approximation in the case where magnetic field is stronger than pseudomagnetic field. We will use the notation of Refs.[23,24]

$$u_0 = \frac{G_{int}}{2\pi l^2}, \quad u_z = \frac{g_{zz}}{2\pi l^2}, \quad u_{\perp} = \frac{g_{\perp z}}{2\pi l^2}. \quad (28)$$

The gap equation in the LLL approximation is obtained from Eq.(26) by replacing the full fermion Green's function $G^{(5)}$ with $G_{LLL}^{(5)}$ and multiplying both sides by the LLL projector $(1 + s_{12} s_{\perp})/2$ (for specificity, in what follows, we take $s_{\perp} = +$). It is easy to see that in the LLL approximation twelve parameters μ_{ν} , $\tilde{\mu}_{\nu}$ and Δ_{ν} , $\tilde{\Delta}_{\nu}$ enter in combinations $s_0(\mu_{\nu} - \Delta_{\nu}) - (\tilde{\mu}_{\nu} - \tilde{\Delta}_{\nu})$. Therefore, we have only six independent variables $\mu_{\nu} - \Delta_{\nu}$ and $\tilde{\mu}_{\nu} - \tilde{\Delta}_{\nu}$. Without loss of generality we can put $\mu_{\nu} = \tilde{\mu}_{\nu} = 0$ so that $m_{\nu} = 0$ and we are left only with parameters d_{ν} . Then the gap equation takes the following form:

$$-d_{\nu}(s_0) \sigma_{\nu} + s_0 \epsilon_Z \sigma_z = - (1 - s_0 b_5) \frac{1}{2} (u_0 + u_z) \left[\frac{d_i(s_0) \sigma_i}{E(s_0)} \theta(E(s_0) - |d_0(s_0)|) + \text{sgn}(d_0(s_0)) \theta(|d_0(s_0)| - E(s_0)) \right] \\ + (1 + s_0 b_5) u_{\perp} \left[\frac{d_i(-s_0) \sigma_i}{E(-s_0)} \theta(E(-s_0) - |d_0(-s_0)|) + \text{sgn}(d_0(-s_0)) \theta(|d_0(-s_0)| - E(-s_0)) \right] \\ + u_z \sum_{s'_0} (1 - s'_0 b_5) \text{sgn}(d_0(s'_0)) \theta(|d_0(s'_0)| - E(s'_0)), \quad (29)$$

where magnetic length $l = \sqrt{\hbar c/|eB_\perp|}$ and $b_5 = B_5/B_\perp$. We find the following solutions of the gap equation (29) (solutions in the case of purely magnetic field are considered in Appendix B 1):

(i) Ferromagnetic (F) solution:

$$\tilde{\Delta}_0 = \Delta_0 = \tilde{\Delta}_x = \Delta_x = 0, \quad \tilde{\Delta}_z = \mp \frac{b_5}{2}(u_0 + u_z - 2u_\perp), \quad \Delta_z = \epsilon_Z \pm \frac{1}{2}(u_0 + u_z + 2u_\perp). \quad (30)$$

This solution exists for $|\tilde{\Delta}_z| < |\Delta_z|$. Using Eqs.(9) and (27), it is easy to check that, for $b_5 \rightarrow 0$, this solution is characterized by the unique order parameter $\langle \Psi^\dagger \sigma_z \Psi \rangle$ which defines uniform magnetization. According to Eq.(7), the corresponding term $\Delta_z \sigma_z \gamma^3 \gamma^5$ in the inverse full propagator describes the Haldane-type mass antisymmetric in spin.

(ii) Antiferromagnetic (AF) solution:

$$\tilde{\Delta}_0 = \Delta_0 = \tilde{\Delta}_x = \Delta_x = 0, \quad \tilde{\Delta}_z = \pm \frac{1}{2}(u_0 + u_z - 2u_\perp), \quad \Delta_z = \epsilon_Z \mp \frac{b_5}{2}(u_0 + u_z + 2u_\perp). \quad (31)$$

This solution exists for $|\tilde{\Delta}_z| > |\Delta_z|$. If we neglect Δ_z compared to $\tilde{\Delta}_z$, the unique order parameter characterizing this solution is $\langle \bar{\Psi} \sigma_z \Psi \rangle$ which defines staggered magnetization. Obviously, the term $\tilde{\Delta}_z \sigma_z$ in the inverse full propagator (7) corresponds to the Dirac-type mass antisymmetric in spin.

(iii) Canted antiferromagnetic (CAF) solution:

$$\begin{aligned} \tilde{\Delta}_0 = \Delta_0 = \Delta_x = 0, \quad \tilde{\Delta}_x &= \pm \frac{1}{2} \sqrt{\left(1 - \frac{b_5^2}{\cos^2 \theta}\right)} (u_0 + u_z - 2u_\perp) \sin \theta, \\ \Delta_z &= \frac{\cos \theta}{2} (u_0 + u_z - 2u_\perp), \quad \tilde{\Delta}_z = -\frac{b_5}{2 \cos \theta} (u_0 + u_z - 2u_\perp), \quad \cos \theta = -\frac{\epsilon_Z}{2u_\perp}. \end{aligned} \quad (32)$$

This solution exists when $\tilde{\Delta}_x$ is real. For $b_5 \rightarrow 0$, this solution is characterized by two nonzero order parameters. They are the staggered magnetization in the x direction $\langle \bar{\Psi} \sigma_x \Psi \rangle$ and the uniform magnetization $\langle \Psi^\dagger \sigma_z \Psi \rangle$ in the z direction. It is important that the order parameter $\langle \bar{\Psi} \sigma_x \Psi \rangle$ can not be transformed into $\langle \bar{\Psi} \sigma_z \Psi \rangle$ by means of a rotation in spin space without inducing the uniform magnetization in the y direction.

(iv) Charge density wave (CDW) solution:

$$\tilde{\Delta}_x = \Delta_x = \tilde{\Delta}_z = 0, \quad \Delta_z = \epsilon_Z, \quad \tilde{\Delta}_0 = \pm \frac{1}{2}(u_0 - 3u_z - 2u_\perp), \quad \Delta_0 = \mp \frac{b_5}{2}(u_0 + u_z + 2u_\perp). \quad (33)$$

For $b_5 \rightarrow 0$, the order parameter which characterizes this solution is $\langle \bar{\Psi} \Psi \rangle$. The corresponding term $\tilde{\Delta}_0$ in the inverse full propagator (7) describes the Dirac mass.

It is easy to check that for $b_5 \neq 0$ pseudomagnetic field induces additional staggered magnetization $\langle \bar{\Psi} \sigma_z \Psi \rangle \sim b_5$ in the F solution, and vice versa, additional uniform magnetization $\langle \Psi^\dagger \sigma_z \Psi \rangle \sim b_5$ in the AF solution. As to the CAF solution, pseudomagnetic field produces additional staggered magnetization in the z direction. Pseudomagnetic field leads also to the generation of the Haldane mass in the CDW solution in addition to the Dirac mass.

The carrier density for strained graphene in the LLL approximation for $|B_\perp| > |B_5|$ is given by

$$\rho = \frac{1}{2\pi l^2} \sum_{s_0} (1 - s_0 b_5) \operatorname{sgn}(\mu_L(s_0)) \theta(|\mu_L(s_0)| - E(s_0)), \quad (34)$$

where $\mu_L(s_0) = -(s_0 \tilde{\Delta}_0 + \Delta_0)$ and $E(s_0) = \sqrt{(s_0 \tilde{\Delta}_x + \Delta_x)^2 + (s_0 \tilde{\Delta}_z + \Delta_z)^2}$. One can check that the carrier density ρ equals zero for the F, AF, and CAF solutions, whereas for the CDW state ρ is nonzero, thus prohibiting it. It is easy to show that for $B_5 \rightarrow 0$ the density $\rho_{CDW} \sim B_5$. Consequently, for $B_5 = 0$, the CDW solution becomes admissible and coincides with the corresponding solution in the case of purely magnetic field obtained in Appendix B 1. Clearly, the F, AF, CAF solutions for $B_5 = 0$ also reduce to those found in Appendix B 1.

B. $|B_{\perp}| < |B_5|$

Similarly to the previous subsection it is more convenient in the case $|b_5| > 1$ to use the following parameters rather than the coupling constants G_{int} , g_{zz} , and $g_{\perp\perp}$:

$$u_{05} = \frac{G_{int}}{2\pi l_5^2}, \quad u_{z5} = \frac{g_{zz}}{2\pi l_5^2}, \quad u_5 = \frac{g_{\perp\perp}}{2\pi l_5^2}, \quad (35)$$

where $l_5 = \sqrt{\hbar c / |eB_5|}$ and for specificity we take $eB_5 > 0$. The gap equation in the LLL approximation is obtained from Eq.(26) by replacing the full fermion Green's function $G^{(5)}$ with $G_{LLL}^{(5)}$ and multiplying both sides by the LLL projector $(1 - s_0)/2$. This time twelve parameters μ_ν , $\tilde{\mu}_\nu$ and Δ_ν , $\tilde{\Delta}_\nu$ enter in combinations $(\mu_\nu + \tilde{\Delta}_\nu) + s_{12}(\tilde{\mu}_\nu - \Delta_\nu)$. Therefore, we have only six independent variables $\mu_\nu + \tilde{\Delta}_\nu$ and $\tilde{\mu}_\nu - \Delta_\nu$. Without loss of generality we can put $\mu_\nu = \tilde{\mu}_\nu = 0$ so that $m_\nu = 0$, and we are left only with parameters d_ν .

By making use of $m_\nu = 0$ and constricting the propagator on the $s_0 = -$ subspace, we obtain the following equation for parameters d_ν :

$$\begin{aligned} -d_\nu(s_{12})\sigma_\nu - \epsilon_Z\sigma_z = & - (1 + s_{12}b_5^{-1})\frac{1}{2}(u_{05} + u_{z5}) \left[\frac{d_i(s_{12})\sigma_i}{E(s_{12})}\theta(E(s_{12}) - |d_0(s_{12})|) + \text{sgn}(d_0(s_{12}))\theta(|d_0(s_{12})| - E(s_{12})) \right] \\ & - (1 - s_{12}b_5^{-1})2u_5 \left[\frac{d_i(-s_{12})\sigma_i}{E(-s_{12})}\theta(E(-s_{12}) - |d_0(-s_{12})|) + \text{sgn}(d_0(-s_{12}))\theta(|d_0(-s_{12})| - E(-s_{12})) \right] \\ & + u_{z5} \sum_{s'_{12}} (1 + s'_{12}b_5^{-1}) \text{sgn}(d_0(s'_{12})) \theta(|d_0(s'_{12})| - E(s'_{12})), \end{aligned} \quad (36)$$

where $d_\nu = \tilde{\Delta}_\nu - s_{12}\Delta_\nu$ and $E(s_{12}) = \sqrt{d_x^2 + d_z^2}$.

We find the following solutions of the above gap equation (solutions in the case of purely pseudomagnetic field are considered in Appendix B 2):

(i) F solution:

$$\tilde{\Delta}_0 = \Delta_0 = \tilde{\Delta}_x = \Delta_x = 0, \quad \tilde{\Delta}_z = -\epsilon_Z \mp \frac{1}{2b_5}(u_{05} + u_{z5} + 4u_5), \quad \Delta_z = \pm \frac{1}{2}(u_{05} + u_{z5} - 4u_5). \quad (37)$$

This solution exists for $|\tilde{\Delta}_z| < |\Delta_z|$.

(ii) AF solution:

$$\tilde{\Delta}_0 = \Delta_0 = \tilde{\Delta}_x = \Delta_x = 0, \quad \tilde{\Delta}_z = -\epsilon_Z \pm \frac{1}{2}(u_{05} + u_{z5} + 4u_5), \quad \Delta_z = \mp \frac{1}{2b_5}(u_{05} + u_{z5} - 4u_5). \quad (38)$$

This solution exists for $|\tilde{\Delta}_z| > |\Delta_z|$.

(iii) CAF solution:

$$\begin{aligned} \tilde{\Delta}_0 = \Delta_0 = \tilde{\Delta}_x = 0, \quad \Delta_x = & \pm \sqrt{(1 - z^2) \left(1 - \frac{1}{b_5^2 z^2}\right)} \frac{1}{2}(u_{05} + u_{z5} - 4u_5), \\ \tilde{\Delta}_z = \frac{z}{2}(u_{05} + u_{z5} - 4u_5), \quad \Delta_z = & -\frac{1}{2b_5 z}(u_{05} + u_{z5} - 4u_5), \quad z = \frac{\epsilon_Z}{4u_5}. \end{aligned} \quad (39)$$

This solution exists only when Δ_x is real. According to the analysis performed in Appendix B 2, the CAF solution is absent in the case where only pseudomagnetic field is present. Therefore, the question arises what happens with the CAF solution found here as $B_{\parallel} = 0$ and $B_{\perp} \rightarrow 0$. Obviously, $\tilde{\Delta}_z$ vanishes in this limit because z is proportional to ϵ_Z and tends to zero. On the other hand, $b_5 z$ does not depend on B_{\perp} and, therefore, is not sensitive to the limit $B_{\perp} \rightarrow 0$. Furthermore, the Hamiltonian of the system in the absence of magnetic field is invariant with respect to $SU(2)$ spin rotations because the Zeeman term vanishes in this case. Then

solutions with different components Δ_i ($i = x, y, z$) in $\Delta = \Delta_x \sigma_x + \Delta_y \sigma_y + \Delta_z \sigma_z$ in ansatz (7) but with the same $\sqrt{\Delta_x^2 + \Delta_y^2 + \Delta_z^2}$ are physically equivalent because they can be easily connected by means of appropriate $SU(2)$ spin rotations. It is not difficult to check that $\sqrt{\Delta_x^2 + \Delta_z^2}$ for the CAF solution (39) equals $|\Delta_z|$ of the F solution (37) as well as $|\Delta_z|$ of the F solution (B11) in the case where only pseudomagnetic field is present. Thus, the F and CAF solutions found in this subsection are physically equivalent if magnetic field is absent.

(iv) QAH solution:

$$\tilde{\Delta}_x = \Delta_x = \Delta_z = 0, \quad \tilde{\Delta}_z = -\epsilon_Z, \quad \tilde{\Delta}_0 = \mp \frac{1}{2b_5}(u_{05} - 3u_{z5} + 4u_5), \quad \Delta_0 = \pm \frac{1}{2}(u_{05} + u_{z5} - 4u_5). \quad (40)$$

Using Eq.(27), we find that the carrier density for strained graphene in the LLL approximation equals

$$\rho = \frac{1}{2\pi l_5^2} \sum_{s_{12}} (1 + s_{12} b_5^{-1}) \text{sgn}(\mu_L(s_{12})) \theta(|\mu_L(s_{12})| - E(s_{12})), \quad (41)$$

where $\mu_L(s_{12}) = \tilde{\Delta}_0 - s_{12}\Delta_0$ and $E(s_{12}) = \sqrt{(\tilde{\Delta}_x - s_{12}\Delta_x)^2 + (\tilde{\Delta}_z - s_{12}\Delta_z)^2}$. For the F, AF, and CAF solutions, the carrier density equals zero while it is nonzero for the QAH solution. Thus, the QAH state is not realized for $B_\perp \neq 0$. For $B_\perp \rightarrow 0$,

$$\rho_{QAH} \simeq -\frac{\text{sgn}\Delta_0}{\pi\hbar c} eB_\perp. \quad (42)$$

Therefore, for $B_\perp = 0$, the QAH solution becomes admissible and coincides with the corresponding solution in Appendix B2. Other solutions also reduce to those in Appendix B2 if $B_\parallel = 0$ and $B_\perp = 0$.

V. PHASE DIAGRAM OF $\nu = 0$ QH STATES IN MAGNETIC AND PSEUDOMAGNETIC FIELDS

We found above several solutions of the gap equation for quasiparticles in graphene in magnetic and pseudomagnetic fields. In order to determine which of these solutions is the ground state, we should calculate their energy densities and then find out the phase diagram of the system. We used the Baym-Kadanoff formalism⁴³ in order to calculate the energy density Ω of the system:

$$\begin{aligned} \Omega = & -\frac{1}{4\pi\hbar c} \sum_{s_0 s_{12}} |eB_\perp - s_0 s_{12} eB_5| \left[\left(E + \epsilon_Z \frac{s_0 d_z - m_z}{E} \right) \theta(E - |\mu_L|) + |d_0 - s_0 m_0| \theta(|\mu_L| - E) \right] \\ & \times \frac{1 + s_{12} \text{sgn}(eB_\perp - s_0 s_{12} eB_5)}{2}, \end{aligned} \quad (43)$$

where $m_{0,z}, d_{0,z}, \mu_L$, and E are functions of discrete variables s_0, s_{12} (see Eqs.(20),(21) and definitions of $m_{0,z}, d_{0,z}$ after Eq.(16)). The derivation of the energy density Ω is given in Appendix C and we retained in Eq.(43) only the contribution due to the lowest Landau level. Therefore, our analysis is valid when the magnitude of dynamically generated gaps is much less than the maximum of Landau gaps $\sqrt{2\hbar v_F^2 |eB_\perp|/c}$ or $\sqrt{2\hbar v_F^2 |eB_5|/c}$.

By making use of the energy density (43) and the solutions found in Sec.IV, we easily calculate the following energy densities for the solutions in the case $|b_5| < 1$:

$$\Omega_F = \frac{|u_\perp| \mp \epsilon_Z}{\pi l^2} - C_<, \quad \Omega_{AF} = \frac{|u_\perp| b_5^2 \pm b_5 \epsilon_Z}{\pi l^2} - C_<, \quad \Omega_{CAF} = -\frac{\epsilon_Z^2}{4|u_\perp| \pi l^2} - C_<, \quad C_< = \frac{(1 + b_5^2)(u_0 + u_z - 2u_\perp)}{4\pi l^2}, \quad (44)$$

where signs in the expressions for Ω_F and Ω_{AF} correlate with the corresponding ones in solutions (30) and (31). These energy densities in the nonstrained limit equal up to a constant to the corresponding energies found in Refs.[23,24]. For $|b_5| > 1$, we have

$$\Omega_F = -\frac{2u_5 b_5^{-2} \pm \epsilon_Z b_5^{-1}}{\pi l_5^2} - C_>, \quad \Omega_{AF} = -\frac{2u_5 \mp \epsilon_Z}{\pi l_5^2} - C_>, \quad \Omega_{CAF} = \frac{\epsilon_Z^2}{8u_5 \pi l_5^2} - C_>, \quad C_> = \frac{(1 + b_5^{-2})(u_{05} + u_{z5} - 4u_5)}{4\pi l_5^2}, \quad (45)$$

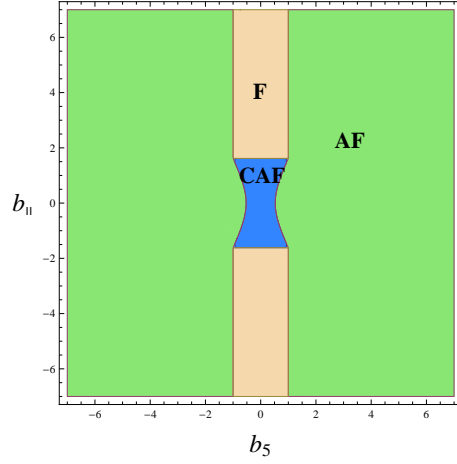


FIG. 1: (Color online) The phase diagram of the $\nu = 0$ QH states in graphene in the plane (b_{\parallel}, b_5) for $g_{\perp\perp} > 0$. The blue color represents the CAF state, green - AF state, and yellow - F state. This diagram is obtained for $B_{\perp} = 20 T$, $u_{\perp} = -13 K$, $2|e|g_{\perp\perp}/(\mu_B\pi\hbar c) = 2.8$, and $\epsilon_Z = 13.4\sqrt{1 + b_{\parallel}^2} K$.

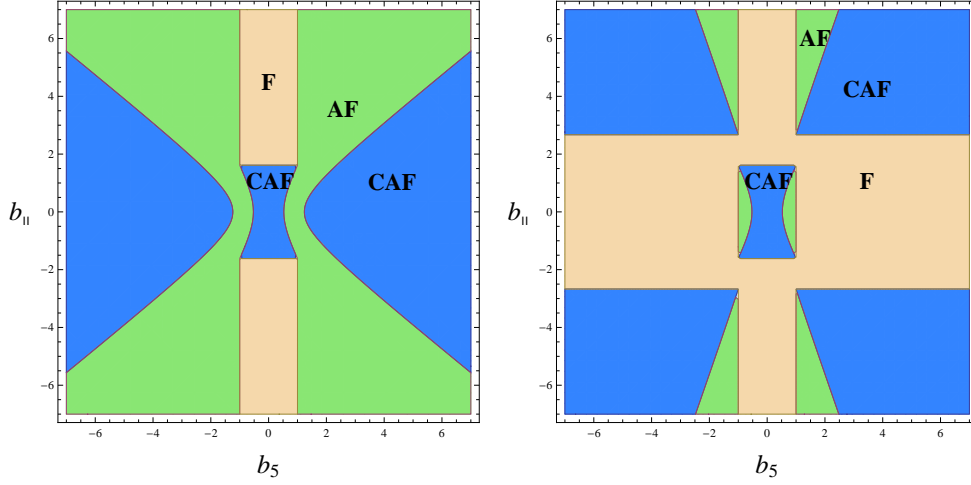


FIG. 2: (Color online) The phase diagram of the $\nu = 0$ QH states in graphene in the plane (b_{\parallel}, b_5) for $-\mu_B\pi\hbar c/(2|e|) < g_{\perp\perp} < 0$ (left panel) and $g_{\perp\perp} < -\mu_B\pi\hbar c/(2|e|)$ (right panel). The blue color represents the CAF state, green - AF state, and yellow - F state. These diagrams similarly to Fig.1 are obtained for $B_{\perp} = 20 T$, $u_{\perp} = -13 K$, and $\epsilon_Z = 13.4\sqrt{1 + b_{\parallel}^2} K$. For the left panel, $2|e|g_{\perp\perp}/(\mu_B\pi\hbar c) = -0.8$, whereas $2|e|g_{\perp\perp}/(\mu_B\pi\hbar c) = -2.8$ for the right panel.

where signs in the expressions for Ω_F and Ω_{AF} correlate with the corresponding ones in solutions (37) and (38). The terms $C_{<}$ and $C_{>}$ describe a common shift in energy density for three solutions, therefore, they are not important for determining the ground state. Hence the energy density depends only on two essential four-fermion coupling constants $g_{\perp z}$ and $g_{\perp\perp}$ (related to u_{\perp} and u_5 , respectively).

Using the energy densities Eqs.(44) and (45), we find the phase diagram of the $\nu = 0$ QH states in graphene in constant magnetic and pseudomagnetic fields. More precisely, we fix the value of perpendicular magnetic field B_{\perp} and study the phase diagram in the plane (b_{\parallel}, b_5) , where $b_{\parallel} = B_{\parallel}/B_{\perp}$ and $b_5 = B_5/B_{\perp}$. In our analysis, following Kharitonov²³, we assume that $u_{\perp} < 0$. Then for $2|u_{\perp}| > \epsilon_Z$ (recall that $\epsilon_Z = \mu_B|B_{\perp}|\sqrt{1 + b_{\parallel}^2}$), we find that the phase diagram depends on coupling constant $g_{\perp\perp}$.

The simplest phase diagram is realized for positive $g_{\perp\perp}$, which we plot in Fig.1. The CAF solution is found to be the ground state of the system in the region defined by $|b_5| < \epsilon_Z(b_{\parallel})/2|u_{\perp}| < 1$, where this solution exists. The side borders of the region with the CAF solution are determined from the condition $|b_5| = \cos\theta = \epsilon_Z(b_{\parallel})/(2|u_{\perp}|)$. This makes the central blue regions, where the CAF state is realized, look like biconcave lens. The top and bottom borders of the region with the CAF solution are determined from the condition $\cos\theta = \epsilon_Z(b_{\parallel})/(2|u_{\perp}|) = 1$.

The ferromagnetic solution with the minus sign in Eq.(44) is the ground state for $|b_{||}| > b_{||}^{cr}$ and $|b_5| < 1$, where $b_{||}^{cr}$ is determined by $\epsilon_Z(b_{||}^{cr}) = 2|u_{\perp}|$, and the AF solution is the most preferable solution for the regions $|b_5| > 1$ and $|b_{||}| < b_{||}^{cr}$, $1 > |b_5| > \epsilon_Z(b_{||})/2|u_{\perp}|$. As to the AF solution, plus and minus sign for it in Eq.(44) is preferable for $b_5 < 0$ and $b_5 > 0$, respectively. The regions of the CAF, F, and AF states are shown in Fig.1 by blue, yellow, and green colors, respectively.

The phase diagram of the system is somewhat more complicated for negative $g_{\perp\perp}$. There are two qualitatively different cases, namely, $-\mu_B\pi\hbar c/(2|e|) < g_{\perp\perp} < 0$ and $g_{\perp\perp} < -\mu_B\pi\hbar c/(2|e|)$. The corresponding phase diagrams are plotted in the left and right panels of Fig.2, respectively, where like in Fig.1 the blue color represents the CAF state, yellow - F state, and green - AF state. Note the symmetry of the phase diagrams with respect to the change $b_5 \rightarrow -b_5$ and $b_{||} \rightarrow -b_{||}$. The main difference of the phase diagram in the left panel of Fig.2 compared to that in Fig.1 is the appearance of two additional regions, where the CAF state is realized as the ground state of the system. The reason for this is that the terms with u_5 in the energy densities of the AF and CAF solutions (45) for $|b_5| > 1$ are of different sign. Therefore, for $g_{\perp\perp} > 0$, the energy density of the AF state is smaller than that of the CAF state. The situation changes for $g_{\perp\perp} < 0$, where the energy density of the CAF state is smaller than that of the AF state for sufficiently small $b_{||}$. As $b_{||}$ increases, the CAF state ceases to exist for $\epsilon_Z > |4u_5|$ and transforms into the AF state. The side borders of two regions with the CAF solution in the left panel in Fig.2 are determined by the condition $(\mu_B\pi\hbar c/(2|e||g_{\perp\perp}|))\sqrt{1+b_{||}^2} = |b_5|$.

For $g_{\perp\perp} < -\mu_B\pi\hbar c/(2|e|)$, the phase diagram becomes even more complicated. Though in this case for $|b_5| > 1$ the CAF solution is also preferable in every point where it exists, this region is now separated in four detached parts. The CAF-AF borders are analogously determined by the condition $(\mu_B\pi\hbar c/(2|e||g_{\perp\perp}|))\sqrt{1+b_{||}^2} = |b_5|$. The CAF-F borders are constant in $b_{||}$ and determined from the condition $(2|e||g_{\perp\perp}|/(\mu_B\pi\hbar c)) = \sqrt{1+b_{||}^2}$. The F solution is more preferable than the AF solution for small $b_{||}$ and $|b_5| > 1$ as is seen from the energy densities in Eq.(45).

It is instructive to compare the obtained results with those in Refs.[23,24] where purely magnetic field was considered. The case of purely magnetic field corresponds to the line $b_5 = 0$ in our phase diagrams. According to Figs.1 and 2, there is the continuous phase transition from the CAF state to the F state as parallel magnetic field $B_{||}$ increases that agrees with Kharitonov's findings.

VI. SUMMARY AND DISCUSSIONS

In the present work, we studied the $\nu = 0$ quantum Hall states in strained monolayer graphene under tilted external magnetic field in the presence of local Coulomb and other local four-fermion interactions, which, in general, break the approximate spin-valley SU(4) symmetry of the low-energy electron Hamiltonian of graphene. Solving the gap equation in the LLL approximation, we found a rich phase diagram where different QH states, the ferromagnetic, antiferromagnetic, and canted antiferromagnetic, compete when we change parallel magnetic field $B_{||}$ and pseudomagnetic field B_5 (we keep perpendicular magnetic field B_{\perp} fixed and rather large). For zero strain, these states are characterized by the nontrivial order parameters $\Psi^{\dagger}\sigma_z\Psi$, $\bar{\Psi}\sigma_z\Psi$, and $\bar{\Psi}\sigma_x\Psi$ and $\Psi^{\dagger}\sigma_z\Psi$, respectively. In the presence of pseudomagnetic field these order parameters gain an admixture of uniform staggered magnetization or uniform magnetization in the z direction.

Assuming that the strength of the Coulomb interaction is larger than all other local interactions, we found an essential dependence of the phase diagram only on two four-fermion couplings $g_{\perp z}$ and $g_{\perp\perp}$, which appear in the low-energy effective Hamiltonian (2). Our main results are accumulated in Figs.1 and 2. For negative coupling $g_{\perp z}$ we found that the canted antiferromagnetic state is always preferable in the center of all figures, i.e., for not too large values of $B_{||}$ and B_5 . When $B_{||}$ and B_5 increase, the ferromagnetic, antiferromagnetic, and canted antiferromagnetic states are realized as the ground state of the system depending on the values of $B_{||}$, B_5 .

The particular case of purely magnetic field corresponds to the line $B_5 = 0$ in our Figs.1 and 2 where there is a phase transition from the CAF state to the F state as parallel magnetic field $B_{||}$ increases that agrees with Kharitonov's findings.^{23,24} In the case of purely pseudomagnetic field considered in Appendix B 2, we find that the F and QAH solutions for $g_{\perp\perp} < 0$ have the lowest and equal energy densities. Since these solutions are described by Haldane-type masses, our results agree with the findings in Ref.[20], where it was shown that pseudomagnetic field catalyses the generation of the Haldane mass. On the hand, for $g_{\perp\perp} > 0$, the AF state with Dirac-type mass is the most preferable. These results and those obtained in Sec.V show that the structure of the phase diagrams in Figs. 1 and 2 is sensitive to the sign and the strength of four-fermion coupling $g_{\perp\perp}$ as well as coupling $g_{\perp z}$.

In our analysis, we ignored boundaries of graphene. However, it is known that they may play an essential role in strained graphene. A novel magnetic ground state, where the Neel and ferromagnetic orders coexist, was reported for the Hubbard Hamiltonian in strained graphene in Ref.[44]. Whereas the Neel order takes the same sign through the

entire system, the magnetization at the boundary takes the opposite sign from the bulk. Since the total magnetization vanishes, the magnetic ground state is edge-compensated antiferromagnet.

In conclusion, strained graphene in a magnetic field provides a unique opportunity to observe various symmetry breaking phases. Further progress in achieving strain induced pseudomagnetic fields, especially uniform pseudomagnetic fields, might allow one to probe experimentally the obtained phase diagram. As for the future, it would be interesting to extend the results of the present paper beyond the neutral point with the filling factor $\nu = 0$ and describe the quantum Hall states with other filling factors.

VII. ACKNOWLEDGMENTS

We are grateful to S.G. Sharapov for useful suggestions and discussions. The work of E.V.G. and V.P.G. was supported partially by the European IRSES Grant No. SIMTECH No. 246937 and by the Program of Fundamental Research of the Physics and Astronomy Division of the NAS of Ukraine.

Appendix A: Quasiparticle propagator: Expansion over LLs

For the Fourier transform in time of the full propagator $G(u, u')$ in Eq. (8) we can write

$$\begin{aligned} G(\omega, \mathbf{r}, \mathbf{r}') &= i \langle \mathbf{r} | [(\omega + m)\gamma^0 - v_F(\boldsymbol{\pi} \cdot \boldsymbol{\gamma}) - d]^{-1} | \mathbf{r}' \rangle = i \langle \mathbf{r} | [(\omega + m)\gamma^0 - v_F(\boldsymbol{\pi} \cdot \boldsymbol{\gamma}) + d] \\ &\times [((\omega + m)\gamma^0 - v_F(\boldsymbol{\pi} \cdot \boldsymbol{\gamma}) - d) ((\omega + m)\gamma^0 - v_F(\boldsymbol{\pi} \cdot \boldsymbol{\gamma}) + d)]^{-1} | \mathbf{r}' \rangle \\ &= i [W - v_F(\boldsymbol{\pi}_r \cdot \boldsymbol{\gamma})] \langle \mathbf{r} | (\mathcal{M} - v_F^2 \boldsymbol{\pi}^2 - ieB_\perp (\hbar v_F^2/c) \gamma^1 \gamma^2)^{-1} | \mathbf{r}' \rangle, \end{aligned} \quad (\text{A1})$$

where $m = \mu + i\gamma^0 \gamma^1 \gamma^2 \tilde{\mu}$, $d = \tilde{\Delta} - i\gamma^0 \gamma^1 \gamma^2 \Delta$, the matrices $\mu, \tilde{\mu}, \Delta, \tilde{\Delta}$ are defined after Eq.(7), and matrices W and \mathcal{M} are

$$W = (\omega + m)\gamma^0 + d, \quad m = m_\nu \sigma_\nu, \quad d = d_\nu \sigma_\nu, \quad \nu = 0, x, z, \quad (\text{A2})$$

$$\mathcal{M} = c + c_i \sigma_i, \quad i = x, y, z, \quad (\text{A3})$$

with

$$\begin{aligned} c &= \omega^2 + 2\omega m_0 + m_\nu^2 - d_\nu^2, \quad c_x = 2(\omega m_x + m_0 m_x - d_0 d_x), \\ c_y &= 2i\gamma^0 (d_x m_z - d_z m_x), \quad c_z = 2(\omega m_z + m_0 m_z - d_0 d_z). \end{aligned} \quad (\text{A4})$$

Our aim is to find an expression for the propagator (A1) as an expansion over LLs (we follow below the consideration in Appendix A in Ref.[27]). The operator $\boldsymbol{\pi}^2$ has well known eigenvalues $(2n + 1)\hbar|eB_\perp|/c$ with $n = 0, 1, 2, \dots$ and its normalized wave functions in the Landau gauge $\mathbf{A} = (0, B_\perp x)$ are

$$\psi_{np}(\mathbf{r}) = \frac{1}{\sqrt{2\pi l}} \frac{1}{\sqrt{2^n n! \sqrt{\pi}}} H_n \left(\frac{x}{l} + pl \right) e^{-\frac{1}{2l^2}(x+pl)^2} e^{ipy}, \quad (\text{A5})$$

where $H_n(x)$ are the Hermite polynomials and $l = \sqrt{\hbar c/|eB_\perp|}$ is the magnetic length. These wave functions satisfy the conditions of normalizability

$$\int d^2r \psi_{np}^*(\mathbf{r}) \psi_{n'p'}(\mathbf{r}) = \delta_{nn'} \delta(p - p'), \quad (\text{A6})$$

and completeness

$$\sum_{n=0}^{\infty} \int_{-\infty}^{\infty} dp \psi_{np}^*(\mathbf{r}) \psi_{np}(\mathbf{r}') = \delta(\mathbf{r} - \mathbf{r}'). \quad (\text{A7})$$

Using the spectral expansion of the unit operator (A7), we obtain

$$\begin{aligned} \langle \mathbf{r} | (\mathcal{M} - v_F^2 \boldsymbol{\pi}^2 - ieB_\perp (\hbar v_F^2/c) \gamma^1 \gamma^2)^{-1} | \mathbf{r}' \rangle &= \frac{1}{2\pi l^2} \exp \left(-\frac{(\mathbf{r} - \mathbf{r}')^2}{4l^2} - i \frac{(x + x')(y - y')}{2l^2} \right) \\ &\times \sum_{n=0}^{\infty} \frac{1}{\mathcal{M} - (2n + 1)(\hbar v_F^2/c) |eB_\perp| - i(\hbar v_F^2/c) eB_\perp \gamma^1 \gamma^2} L_n \left(\frac{(\mathbf{r} - \mathbf{r}')^2}{2l^2} \right), \end{aligned} \quad (\text{A8})$$

where we integrated over p by using

$$\int_{-\infty}^{\infty} e^{-x^2} H_m(x+y) H_n(x+z) dx = 2^n \pi^{1/2} m! z^{n-m} L_m^{n-m}(-2yz), \quad (\text{A9})$$

assuming $m \leq n$. Here L_n^α are the generalized Laguerre polynomials, and $L_n \equiv L_n^0$. The matrix $i(\hbar v_F^2/c)eB_\perp \gamma^1 \gamma^2$ has eigenvalues $\pm \hbar v_F^2 |eB_\perp|/c = \pm \epsilon_B^2/2$. Therefore, we have

$$\frac{L_n(\xi)}{\mathcal{M} - (2n+1)(\hbar v_F^2/c)|eB_\perp| - i(\hbar v_F^2/c)eB_\perp \gamma^1 \gamma^2} = \frac{P_- L_n(\xi)}{\mathcal{M} - n\epsilon_B^2} + \frac{P_+ L_n(\xi)}{\mathcal{M} - (n+1)\epsilon_B^2}, \quad (\text{A10})$$

where $\xi = (\mathbf{r} - \mathbf{r}')^2/(2l^2)$ and the projectors P_\pm are

$$P_\pm = \frac{1}{2} [1 \pm i\gamma^1 \gamma^2 \text{sign}(eB_\perp)]. \quad (\text{A11})$$

By redefining $n \rightarrow n-1$ in the second term in Eq. (A10), Eq.(A8) can be rewritten as

$$\langle \mathbf{r} | [\mathcal{M} - v_F^2 \boldsymbol{\pi}^2 - ieB_\perp (\hbar v_F^2/c) \gamma^1 \gamma^2]^{-1} | \mathbf{r}' \rangle = \frac{1}{2\pi l^2} e^{i\Phi(\mathbf{r}, \mathbf{r}')} e^{-\xi/2} \sum_{n=0}^{\infty} \frac{P_- L_n(\xi) + P_+ L_{n-1}(\xi)}{\mathcal{M} - n\epsilon_B^2}, \quad (\text{A12})$$

where $L_{-1} \equiv 0$ by definition and

$$\Phi(\mathbf{r}, \mathbf{r}') = -\frac{(x+x')(y-y')}{2l^2} = -\frac{e}{\hbar c} \int_{\mathbf{r}'}^{\mathbf{r}} dz_i A_i(z) \quad (\text{A13})$$

is the Schwinger phase⁴⁵ which appears due to the noncommutative character of magnetic translations⁴⁶. Since

$$\pi_x e^{i\Phi} = e^{i\Phi} \hbar \left(-i\partial_x - \frac{y-y'}{2l^2} \right), \quad \pi_y e^{i\Phi} = e^{i\Phi} \hbar \left(-i\partial_y + \frac{x-x'}{2l^2} \right), \quad (\text{A14})$$

propagator (A1) can be presented as a product of the phase factor and a translation invariant part $\bar{G}(\omega; \mathbf{r} - \mathbf{r}')$,

$$G(\omega; \mathbf{r}, \mathbf{r}') = e^{i\Phi(\mathbf{r}, \mathbf{r}')} \bar{G}(\omega; \mathbf{r} - \mathbf{r}'), \quad (\text{A15})$$

where

$$\bar{G}(\omega; \mathbf{r} - \mathbf{r}') = i \left[W - \hbar v_F \gamma^1 \left(-i\partial_x - \frac{y-y'}{2l^2} \right) - \hbar v_F \gamma^2 \left(-i\partial_y + \frac{x-x'}{2l^2} \right) \right] \frac{e^{-\xi/2}}{2\pi l^2} \sum_{n=0}^{\infty} \frac{P_- L_n(\xi) + P_+ L_{n-1}(\xi)}{\mathcal{M} - n\epsilon_B^2} \quad (\text{A16})$$

The Fourier transform of the translation invariant part of propagator (A16) can be evaluated by performing the integration over the angle,

$$\int_0^{2\pi} d\theta e^{ikr \cos \theta} = 2\pi J_0(kr), \quad (\text{A17})$$

where $J_0(x)$ is the Bessel function, and then using the following formula:

$$\int_0^\infty x e^{-\frac{1}{2}\alpha x^2} L_n \left(\frac{1}{2}\beta x^2 \right) J_0(xy) dx = \frac{(\alpha - \beta)^n}{\alpha^{n+1}} e^{-\frac{1}{2\alpha} y^2} L_n \left(\frac{\beta y^2}{2\alpha(\beta - \alpha)} \right), \quad (\text{A18})$$

valid for $y > 0$ and $\text{Re } \alpha > 0$. We obtain

$$\bar{G}(\omega, \mathbf{k}) = ie^{-k^2 l^2} \sum_{n=0}^{\infty} \frac{(-1)^n D_n(\omega, \mathbf{k})}{\mathcal{M} - n\epsilon_B^2}, \quad (\text{A19})$$

with

$$D_n(\omega, \mathbf{k}) = 2W [P_- L_n(2k^2 l^2) - P_+ L_{n-1}(2k^2 l^2)] + 4\hbar v_F (\mathbf{k} \cdot \boldsymbol{\gamma}) L_{n-1}^1(2k^2 l^2), \quad L_{-1}^\alpha \equiv 0, \quad (\text{A20})$$

describing the n th Landau level contribution.

Appendix B: Solutions of gap equation in purely magnetic or pseudomagnetic field

1. Purely magnetic field

Let us find solutions of the gap equation (24) in the LLL approximation in the case where only magnetic field is present. In this case, the gap equation takes the form:

$$\begin{aligned}
-d_\nu(s_0)\sigma_\nu + s_0\epsilon_Z\sigma_z = & -\frac{1}{2}(u_0 + u_z) \left[\frac{d_i(s_0)\sigma_i}{E(s_0)}\theta(E(s_0) - |d_0(s_0)|) + \text{sgn}(d_0(s_0))\theta(|d_0(s_0)| - E(s_0)) \right] \\
& + u_\perp \left[\frac{d_i(-s_0)\sigma_i}{E(-s_0)}\theta(E(-s_0) - |d_0(-s_0)|) + \text{sgn}(d_0(-s_0))\theta(|d_0(-s_0)| - E(-s_0)) \right] \\
& + u_z \sum_{s'_0} \text{sgn}(d_0(s'_0))\theta(|d_0(s'_0)| - E(s'_0)), \tag{B1}
\end{aligned}$$

where $d_\nu = \tilde{\Delta}_\nu + s_0\Delta_\nu$ and $E = \sqrt{d_x^2 + d_z^2}$. Projecting on the Pauli matrices, we get

$$d_0(s_0) = \frac{1}{2}(u_0 - u_z) \text{sgn}(d_0(s_0)) \theta(|d_0(s_0)| - E(s_0)) - (u_\perp + u_z) \text{sgn}(d_0(-s_0)) \theta(|d_0(-s_0)| - E(-s_0)), \tag{B2}$$

$$d_x(s_0) = \frac{1}{2}(u_0 + u_z) \frac{d_x(s_0)}{E(s_0)}\theta(E(s_0) - |d_0(s_0)|) - u_\perp \frac{d_x(-s_0)}{E(-s_0)}\theta(E(-s_0) - |d_0(-s_0)|), \tag{B3}$$

$$d_z(s_0) - s_0\epsilon_Z = \frac{1}{2}(u_0 + u_z) \frac{d_z(s_0)}{E(s_0)}\theta(E(s_0) - |d_0(s_0)|) - u_\perp \frac{d_z(-s_0)}{E(-s_0)}\theta(E(-s_0) - |d_0(-s_0)|). \tag{B4}$$

These equations define a system of non-linear equations because E is a non-linear function of d_x and d_z . Since G_{int} approximates the Coulomb interaction, which is the strongest electron-electron interaction in graphene, we assume in what follows that $u_0 \gg \epsilon_Z, u_z, u_\perp$. The system of equations (B2)-(B4) has the following solutions which are consistent with the charge neutrality condition for both \pm signs:

(i) F solution:

$$\tilde{\Delta}_0 = \Delta_0 = \tilde{\Delta}_x = \Delta_x = 0, \quad \tilde{\Delta}_z = 0, \quad \Delta_z = \epsilon_Z \pm \frac{1}{2}(u_0 + u_z + 2u_\perp). \tag{B5}$$

(ii) AF solution:

$$\tilde{\Delta}_0 = \Delta_0 = \tilde{\Delta}_x = \Delta_x = 0, \quad \tilde{\Delta}_z = \pm \frac{1}{2}(u_0 + u_z - 2u_\perp), \quad \Delta_z = \epsilon_Z, \tag{B6}$$

which exists for $|\tilde{\Delta}_z| > \epsilon_Z$ that is satisfied automatically since we assumed $u_0 \gg \epsilon_Z, u_z, u_\perp$.

(iii) CAF solution:

$$\begin{aligned}
\tilde{\Delta}_0 = \Delta_0 = 0, \quad \Delta_x = \tilde{\Delta}_z = 0, \quad \cos\theta = -\frac{\epsilon_Z}{2u_\perp}, \\
\tilde{\Delta}_x = \pm \frac{1}{2}(u_0 + u_z - 2u_\perp) \sin\theta, \quad \Delta_z = \frac{1}{2}(u_0 + u_z - 2u_\perp) \cos\theta. \tag{B7}
\end{aligned}$$

The CAF solution exists only for $\epsilon_Z < 2|u_\perp|$.

(iv) CDW solution:

$$\Delta_0 = \Delta_x = \tilde{\Delta}_x = \tilde{\Delta}_z = 0, \quad \Delta_z = \epsilon_Z, \quad \tilde{\Delta}_0 = \pm \frac{1}{2}(u_0 - 3u_z - 2u_\perp). \tag{B8}$$

The ferromagnetic and CAF solutions reproduce solutions obtained in Refs.[23,24]. Note that here like in Sec.V we follow Kharitonov^{23,24} and assume that $u_{\perp} < 0$. In this case, the CAF solution is the ground state of the system for sufficiently small parallel magnetic field.

Since in the present paper we consider the state with zero filling factor, $\nu = 0$, we need to control the carrier density ρ which according to Eqs.(11),(25) in the LLL approximation is given by the expression

$$\rho = \frac{1}{2\pi l^2} \sum_{s_0} \text{sgn}(\mu_L(s_0)) \theta(|\mu_L(s_0)| - E(s_0)), \quad (\text{B9})$$

where $\mu_L(s_0) = -(s_0\tilde{\Delta}_0 + \Delta_0)$ and $E(s_0) = \sqrt{(\tilde{\Delta}_x + s_0\Delta_x)^2 + (\tilde{\Delta}_z + s_0\Delta_z)^2}$. It is easy to check that for all obtained solutions the carrier density ρ vanishes so that the filling $\nu = 0$ is realized. The ground state is determined by the solution with the lowest free energy density. The case of purely magnetic field corresponds to the line $B_5 = 0$ in Figs.1 and 2 in Sec.V. One can see that there is a phase transition from the CAF state to the F state as parallel magnetic field B_{\parallel} increases that agrees with the results obtained by Kharitonov in Refs.[23,24].

2. Purely pseudomagnetic field

In this subsection, we consider solutions of the gap equation (26) in the case where only pseudomagnetic field is present ($B_{\perp} = B_{\parallel} = 0$) retaining only the LLL contribution. Without loss of generality we can put $\mu_{\nu} = \tilde{\mu}_{\nu} = 0$ so that $m_{\nu} = 0$, and we are left only with parameters d_{ν} . Moreover, due to the absence of the Zeeman term the gap equation possesses the SU(2) spin symmetry, so that we can take $d_x = 0$. Therefore, we get the following equation for the parameters d_0 and d_z :

$$\begin{aligned} -d_z(s_{12})\sigma_z - d_0(s_{12}) = & -\frac{1}{2}(u_{05} + u_{z5}) \left[\text{sgn}(d_z(s_{12}))\theta(E(s_{12}) - |d_0(s_{12})|)\sigma_z + \text{sgn}(d_0(s_{12}))\theta(|d_0(s_{12})| - E(s_{12})) \right] \\ & - 2u_5 \left[\text{sgn}(d_z(-s_{12}))\theta(E(-s_{12}) - |d_0(-s_{12})|)\sigma_z + \text{sgn}(d_0(-s_{12}))\theta(|d_0(-s_{12})| - E(-s_{12})) \right] \\ & + u_{z5} \sum_{s'_{12}} \text{sgn}(d_0(s'_{12}))\theta(|d_0(s'_{12})| - E(s'_{12})), \end{aligned} \quad (\text{B10})$$

where $d_{0,z} = \tilde{\Delta}_{0,z} - s_{12}\Delta_{0,z}$ and $E = |d_z|$.

Assuming that $u_{05} \gg u_{z5}, u_5$, we find the following solutions:

(i) F solution:

$$\tilde{\Delta}_0 = \Delta_0 = 0, \quad \tilde{\Delta}_z = 0, \quad \Delta_z = \pm \frac{1}{2}(u_{05} + u_{z5} - 4u_5); \quad (\text{B11})$$

(ii) AF solution:

$$\tilde{\Delta}_0 = \Delta_0 = 0, \quad \tilde{\Delta}_z = \pm \frac{1}{2}(u_{05} + u_{z5} + 4u_5), \quad \Delta_z = 0; \quad (\text{B12})$$

(iii) QAH solution:

$$\tilde{\Delta}_z = \Delta_z = 0, \quad \tilde{\Delta}_0 = 0, \quad \Delta_0 = \pm \frac{1}{2}(u_{05} + u_{z5} - 4u_5). \quad (\text{B13})$$

Note that the CAF solution is no longer present due to the absence of the Zeeman term. For the carrier density we obtain the following expression:

$$\rho = \frac{1}{2\pi l_5^2} \sum_{s_{12}} \text{sgn}(\tilde{\Delta}_0 - s_{12}\Delta_0) \theta\left(|\tilde{\Delta}_0 - s_{12}\Delta_0| - |\tilde{\Delta}_z - s_{12}\Delta_z|\right). \quad (\text{B14})$$

One can check that the condition $\rho = 0$ is satisfied for all obtained solutions. The ground state of the system is determined as the solution with the lowest free energy density (see Sec.V). By making use of the energy density (43) for $B_{\perp} = \epsilon_Z = 0$, we find that the F and QAH solutions for $g_{\perp\perp} < 0$ have the lowest and equal energy densities. According to Eqs.(B11) and (B13), the F and QAH solutions are described by Haldane-type masses. These results agree with the findings in Ref.[20], where it was shown that pseudomagnetic field catalyses the generation of the Haldane mass. On the hand, we find that for $g_{\perp\perp} > 0$ the AF state with Dirac-type mass (B12) is the most preferable. Once again, like in Sec.V, these results show the crucial role of the coupling constant $g_{\perp\perp}$ in the selection of the ground state of the system in a strong pseudomagnetic field.

Appendix C: Free-energy density

The energy density is defined by the following expression $\Omega = -\Gamma/TV$, where TV is a space-time volume. By utilizing the Baym-Kadanoff-Jackiw-Tomboulis) formalism, we find the effective action Γ at its extrema in the mean-field approximation (for details see Ref.[27]):

$$\Gamma = -iT \text{Tr} \left[\ln G^{-1} + \frac{1}{2}(S^{-1}G - 1) \right], \quad (\text{C1})$$

where the trace, logarithm, and product $S^{-1}G$ are taken in the functional sense, $G = \text{diag}(G_+, G_-)$, 1 is the unit operator in both matrix and coordinate sense and the expressions for the free and full propagator are given by Eqs.(6) and (7). Performing the Fourier transform in time, integrating by parts the logarithm term, and omitting the irrelevant surface term, we arrive at the expression (for simplicity in this section we put constants $\hbar = c = 1$):

$$\Gamma = -iT \int_{-\infty}^{\infty} \frac{dw}{2\pi} \text{Tr} \left[-w \frac{\partial G^{-1}(w)}{\partial w} G(w) + \frac{1}{2}(S^{-1}(w)G(w) - 1) \right] \quad (\text{C2})$$

with

$$\frac{\partial G^{-1}(w)}{\partial w} = -i\gamma^0 \delta(\mathbf{r} - \mathbf{r}').$$

The multiplier T came from the functional trace in time, and now Tr contains only spatial integration. By substituting the expression for the Green function (A15) into $\Omega = -\Gamma/TV$, one can see that Schwinger phase Φ goes away and after the Fourier transformation we get for the energy density

$$\begin{aligned} \Omega &= i \int_{-\infty}^{\infty} \frac{dw}{2\pi} \int \frac{d^2k}{(2\pi)^2} \text{tr} \left[i\gamma^0 w \bar{G}(w, \mathbf{k}) + \frac{1}{2} [-i\{(w - \epsilon_Z \sigma_Z)\gamma^0 - v_F(\mathbf{k} \cdot \boldsymbol{\gamma})\} \bar{G}(w; \mathbf{k}) - 1] \right] \\ &= - \int_{-\infty}^{\infty} \frac{dw}{4\pi} \int \frac{d^2k}{(2\pi)^2} \text{tr} \{ [(w + \epsilon_Z \sigma_Z)\gamma^0 + v_F(\mathbf{k} \cdot \boldsymbol{\gamma})] \bar{G}(w; \mathbf{k}) + i \}. \end{aligned} \quad (\text{C3})$$

By making use of the explicit form of the propagator, we calculate the following integrals which contribute to the energy density:

$$\int \frac{d^2k}{(2\pi)^2} \gamma^0 \bar{G}_s(w; \mathbf{k}) = \frac{i|eB|}{2\pi} \sum_{n=0}^{\infty} \gamma^0 W \frac{P_- + P_+ \theta(n - 1/2)}{\mathcal{M} - n\epsilon_B^2}, \quad (\text{C4})$$

$$\int \frac{d^2k}{(2\pi)^2} v_F(\mathbf{k} \cdot \boldsymbol{\gamma}) \bar{G}_s(w; \mathbf{k}) = \frac{i|eB|}{2\pi} \sum_{n=0}^{\infty} \frac{n\epsilon_B^2}{\mathcal{M} - n\epsilon_B^2}, \quad (\text{C5})$$

where in strained case we use the effective magnetic field $B = B_{\perp} - s_0 s_{12} B_5$ in the Landau energy ϵ_B and projectors P_{\pm} .

By dropping an infinite divergent term independent of the physical parameters and normalizing Ω by subtracting its value at $m_{\mu} = d_{\mu} = \epsilon_Z = 0$, we obtain the following expression:

$$\Omega = - \frac{i|eB|}{4\pi} \int_{-\infty}^{\infty} \frac{dw}{2\pi} \text{tr} \sum_{n=0}^{\infty} \left[\frac{(w + \epsilon_Z \sigma_Z)\gamma^0 W (P_- + P_+ \theta(n - 1/2)) + n\epsilon_B^2}{\mathcal{M} - n\epsilon_B^2} - \frac{w^2 (P_- + P_+ \theta(n - 1/2)) + n\epsilon_B^2}{w^2 - n\epsilon_B^2} \right]. \quad (\text{C6})$$

After integrating this expression over frequency and taking trace, we finally arrive at Eq.(43).

¹ X. Li, X. Wang, L. Zhang, S. Lee, and H. Dai, *Science* **319**, 1229 (2008).

² T. Low and F. Guinea, *Nano Letters* **10**, 3551 (2010).

³ J. Lu, A.C. Neto, and K.P. Loh, *Nature Communications* **3**, 823 (2012).

⁴ H. Suzuura and T. Ando, *Phys. Rev. B* **65**, 235412 (2002).

⁵ J.L. Manes, *Phys. Rev. B* **76**, 045430 (2007).

⁶ S.V. Morozov, K.S. Novoselov, M.I. Katsnelson, F. Schedin, D. Jiang, and A.K. Geim, *Phys. Rev. Lett.* **97**, 016801 (2006).

- ⁷ T.O. Wehling, A.V. Balatsky, A.M. Tselik, M.I. Katsnelson, and A.I. Lichtenstein, *Europhys. Lett.* **84**, 17003 (2008).
- ⁸ M.A. Vozmediano, M. Katsnelson, and F. Guinea, *Physics Reports* **496**, 109 (2010).
- ⁹ M.I. Katsnelson, *Graphene: Carbon in two dimensions* (Cambridge University Press, Cambridge, 2012).
- ¹⁰ F. Guinea, M.I. Katsnelson, and A.K. Geim, *Nature Physics* **6**, 30 (2010).
- ¹¹ F. Guinea, A.K. Geim, M.I. Katsnelson, and K.S. Novoselov, *Phys. Rev. B* **81**, 035408 (2010).
- ¹² K.S. Novoselov, A.K. Geim, S.V. Morozov, D. Jaing, M.I. Katsnelson, I.V. Grigorieva, S.V. Dubonos, and A.A. Firsov, *Nature* **438**, 197 (2005); Y. Zhang, Y.-W. Tan, H.L. Störmer, and P. Kim, *Nature* **438**, 201 (2005).
- ¹³ V.P. Gusynin and S.G. Sharapov, *Phys. Rev. Lett.* **95**, 146801 (2005).
- ¹⁴ N.M.R. Peres, F. Guinea, and A.H. Castro Neto, *Phys. Rev. B* **73**, 1254111 (2006).
- ¹⁵ Y. Zhang, Z. Jiang, J.P. Small, M.S. Purewal, Y.-W. Tan, M. Fazlollahi, J.D. Chudow, J.A. Jaszczak, H.L. Stormer, and P. Kim, *Phys. Rev. Lett.* **96**, 136806 (2006).
- ¹⁶ Z. Jiang, Y. Zhang, H.L. Stormer, and P. Kim, *Phys. Rev. Lett.* **99**, 106802 (2007).
- ¹⁷ N. Levy, S.A. Burke, K.L. Meaker, M. Panlasigui, A. Zettl, F. Guinea, A.H. Castro Neto, and M.F. Crommie, *Science* **329**, 544 (2010).
- ¹⁸ E. Prada, P. San-Jose, G. Leon, M.M. Fogler, and F. Guinea, *Phys. Rev. B* **81**, 161402(R) (2010).
- ¹⁹ B. Roy, Z.-X. Hu, and K. Yang, *Phys. Rev. B* **87**, 121408(R) (2013).
- ²⁰ I.F. Herbut, *Phys. Rev. B* **78**, 205433 (2008).
- ²¹ B. Roy and J.D. Sau, *Phys. Rev. B* **90**, 075427 (2014).
- ²² K.K. Gomes, W. Mar, W. Ko, F. Guinea, and H. Manoharan, *Nature* **483**, 306 (2012).
- ²³ M. Kharitonov, *Phys. Rev. B* **85**, 155439 (2012).
- ²⁴ M. Kharitonov, *Phys. Rev. B* **86**, 075450 (2012).
- ²⁵ R. Jackiw and S.-Y. Pi, *Phys. Rev. Lett.* **98**, 266402 (2007).
- ²⁶ B. Roy, *Phys. Rev. B* **84**, 035458 (2012).
- ²⁷ E.V. Gorbar, V.P. Gusynin, V.A. Miransky, and I.A. Shovkovy, *Phys. Rev. B* **78**, 085437 (2008).
- ²⁸ J. Alicea and M.P.A. Fisher, *Phys. Rev. B* **74**, 075422 (2006).
- ²⁹ I. L. Aleiner, D. E. Kharzeev, and A. M. Tselik, *Phys. Rev.* **B6**, 195415 (2007).
- ³⁰ D.V. Khveshchenko, *Phys. Rev. Lett.* **87**, 206401 (2001); **87**, 246802 (2001).
- ³¹ E.V. Gorbar, V.P. Gusynin, V.A. Miransky, and I.A. Shovkovy, *Phys. Rev. B* **66**, 045108 (2002).
- ³² K. Nomura and A.H. MacDonald, *Phys. Rev. Lett.* **96**, 256602 (2006); K. Yang, S. Das Sarma, and A.H. MacDonald, *Phys. Rev. B* **74**, 075423 (2006).
- ³³ M.O. Goerbig, R. Moessner, and B. Doucot, *Phys. Rev. B* **74**, 161407(R) (2006).
- ³⁴ L. Sheng, D.N. Sheng, F.D.M. Haldane, and L. Balents, *Phys. Rev. Lett.* **99**, 196802 (2007).
- ³⁵ V.P. Gusynin, V.A. Miransky, S.G. Sharapov, and I.A. Shovkovy, *Phys. Rev. B* **74**, 195429 (2006).
- ³⁶ I.F. Herbut, *Phys. Rev. B* **75**, 165411 (2007).
- ³⁷ J.-N. Fuchs and P. Lederer, *Phys. Rev. Lett.* **98**, 016803 (2007).
- ³⁸ M. Ezawa, *J. Phys. Soc. Japan* **76**, 094701 (2007).
- ³⁹ K. Yang, *Solid State Commun.* **143**, 27 (2007).
- ⁴⁰ E.V. Gorbar, V.P. Gusynin, and V.A. Miransky, *Low Temp. Phys.* **34**, 790 (2008).
- ⁴¹ M.O. Goerbig, *Rev. Mod. Phys.* **83**, 1193 (2011).
- ⁴² E.V. Gorbar, V.P. Gusynin, V.A. Miransky, and I.A. Shovkovy, *Phys. Scr.* **T 146**, 014018 (2012).
- ⁴³ G. Baym and L.P. Kadanoff, *Phys. Rev.* **124**, 287 (1961); J.M. Cornwall, R. Jackiw, and E. Tomboulis, *Phys. Rev. D* **10**, 2428 (1974).
- ⁴⁴ B. Roy, F.F. Assaad, and I.F. Herbut, *Phys. Rev. X* **4**, 021042 (2014).
- ⁴⁵ J. Schwinger, *Phys. Rev.* **82**, 664 (1951).
- ⁴⁶ J. Zak, *Phys. Rev.* **134**, A1602 (1964).